Desalination and Water Treatment
www.deswater.com

doi: 10.1080/19443994.2015.1058193

57 (2016) 13494–13504
June

Taylor & Francis
Taylor & Francis Group

Photocatalytic degradation of a textile dye in aqueous phase over ZnO nanoparticles embedded in biosilica nanobiostructure

R. Darvishi Cheshmeh Soltani[a,*], A.R. Khataee[b], M. Mashayekhi[a]

[a]*Department of Environmental Health Engineering, School of Health, Arak University of Medical Sciences, 38196-93345 Arak, Iran, Tel. +98 86 33662024; Fax: +98 86 33686443; emails: darvishi@arakmu.ac.ir (R. Darvishi Cheshmeh Soltani), ms.mashayekhi19@yahoo.com (M. Mashayekhi)*

[b]*Research Laboratory of Advanced Water and Wastewater Treatment Processes, Faculty of Chemistry, Department of Applied Chemistry, University of Tabriz, 51666-16471 Tabriz, Iran, Tel. +98 411 3393165; email: a_khataee@tabrizu.ac.ir*

Received 25 December 2014; Accepted 30 May 2015

ABSTRACT

In the present study, ZnO nanoparticles immobilized on biosilica nanobiostructure were used for the photocatalytic degradation of Acid Red 88 (AR88) in aqueous phase. UV-induced ZnO/biosilica nanocomposite (78.84%) was more efficient than visible light-induced ZnO/biosilica nanocomposite (21.87%). The results of UV–vis diffuse reflectance spectra (DRS) indicated that the enhanced UV–vis absorption of the nanocomposite could be attributed to biosilica support. Increasing the adsorbent dosage from 0.1 to 1.5 g/L caused a sharp increase in the decolorization efficiency from 15.30 to 98.54%, respectively, while further increase in the amount of photocatalyst to 2 g/L led to a little drop in the decolorization efficiency, decreasing to 93.63%. Decreasing the initial AR88 concentration from 70 to 10 mg/L enhanced the apparent reaction rate constant (k_{ap}) from 0.0078 to 0.1579 min^{-1} and diminished the consumption of electrical energy (EE_0) from 2,813 to 139 kW h/m^3, respectively. The decolorization and mineralization efficiency of 96.32 and 65.57% were obtained, respectively, thereby confirming an acceptable mineralization of AR88 within 30 min.

Keywords: Photocatalysis; Nanosized ZnO; Siliceous nanobiostructure; Immobilized nanocatalyst; Organic dye

1. Introduction

The release of textile-processing effluents to aqueous environments is very problematic to human health and aquatic life because of toxic and mutagenic properties of the organic dyes [1–4]. Owing to the toxicity of the organic dyes, the decolorization of colored effluents has attracted much more attention worldwide [5]. Biological processes are not proposed for the treatment of colored effluents because of the biological resistance of some organic dyes [6]. Due to the low biodegradability of organic dyes, various physicochemical technologies such as chemical oxidation, adsorption process, ultrafiltration, chemical precipitation, electrochemical processes, and membrane technologies have been applied for removing organic dyes from the aqueous phase [1,3]. Most conventional methods are inefficient in removing organic dyes from wastewaters [7]. In recent years, the application of advanced oxidation process (AOPs) has gained much more attention for the mineralization of refractory

*Corresponding author.

organic compounds such as organic dyes in polluted water due to the generation of hydroxyl radical ($OH^{\bullet}$) as one of the most powerful and non-selective oxidizing agents [8–10]. AOPs include catalytic ozonation, ultrasounds, wet air oxidation, peroxon, Fenton and photo-Fenton processes, radiolysis, electrochemical processes, and photocatalysis [6,11,12]. Among various AOPs, photocatalytic processes based on the semiconductors have been widely used for treating polluted industrial effluents [8,9,12,13]. Photocatalysis is considered as one of the most environmentally friendly AOPs with a high potential to degrade organic contaminants into water and carbon dioxide [6,13]. Among all semiconductors, the application of ZnO, in nanosize can be considered as a promising alternative in photocatalysis due to its wide band gap (3.37 eV), large volume-to-area ratio, low cost, and high potential to adsorb UV irradiation [8,9,13–15]. The generation of $OH^{\bullet}$ during a photocatalytic process equipped with ZnO nanoparticles is illustrated via Eqs. (1) and (2) [8,13,16]:

$$ZnO + hv \rightarrow ZnO\ (e^{-} + h^{+}) \quad (1)$$

$$h^{+} + H_2O \rightarrow H^{+} + OH^{\bullet} \quad (2)$$

The toxic effects of nanostructures like ZnO for aqueous and terrestrial environments have been demonstrated. For instance, ZnO nanoparticles can cause toxicity with LC_{50} of about 2.3 mg/L to the nematode *Caenorhabditis elegans* [16–19]. Therefore, discharging nanomaterials into the environment must be limited. Moreover, the aggregation of suspended nanocatalysts in aqueous solutions has been observed to cause a significant drop in their photocatalytic activity [8]. One effective approach to reduce these problems is to find an appropriate material to be used as a kind of support for the immobilization of nanosized catalysts. The immobilization of semiconductors on an appropriate support can improve their life and reusability potential for the application in consecutive operational runs [20–22]. This approach improves the mechanical strength of the catalyst particles and increases their mass density and retention time in the photoreactor. Besides, immobilization strategy is a necessary stage for the scale up of treatment technologies [3,16]. Therefore, the immobilization of nanosized photocatalysts on the surface of some suitable supports such as silica or alumina has been considered [11,23]. Due to availability and cost efficiency, clay-like supports represent an attractive material for the immobilization of various semiconductors [14,24–26]. Among various clay-like supports, biosilica is a biologically siliceous clay with a porous structure consisting of 87–91% silicone dioxide, which can be used as an alternative support for the immobilization due to its high surface area, together with suitable functional groups, to achieve stable immobilization of nanosized catalysts on it [3,4,21]. Based on the aforementioned advantages, in the present study, ZnO nanoparticles were embedded in biosilica nanobiostructure to mitigate their negative environmental effects and make their application more economical. The main aim of the present investigation was to prepare ZnO nanoparticles embedded in biosilica nanobiostructure and evaluate its photocatalytic activity for the photocatalysis of Acid Red 88 (AR88) as the model organic azo dye. The effect of various operational parameters on the photocatalytic decolorization was evaluated too. Furthermore, the reusability of the photocatalyst and the potential of photocatalyst for the mineralization of AR88 were assessed from an application point of view. To the best of our knowledge, the application of ZnO nanoparticles embedded in biosilica nanobiostructure as the photocatalyst for the photocatalysis of textile dyes has not been reported elsewhere.

2. Materials and methods

2.1. Chemicals

ZnO nanoparticles were purchased from US Research Nanomaterials, USA. The azo dye AR88 (molecular formula: $C_{20}H_{13}N_2O_4SNa$ and molecular weight: 400.38 g/mol) was purchased from Nasaj Sabet Company, Iran and used without any purification. Biosilica nanobiostructure was purchased from Sigma-Aldrich, USA. According to the results of our previous study, the biosilica contains nanoscale crystals and the nanoporous structure [3]. All other chemicals, which were of analytical grade, were obtained from Merck, Germany. The adjustment of solution pH was done via the addition of 0.1 M sodium hydroxide or 0.1 M hydrochloric acid.

2.2. Preparation of the immobilized photocatalyst

ZnO nanoparticles embedded in biosilica nanobiostructure were fabricated as follows: ZnO nanoparticles were dissolved in 50 mL of deionized water to achieve a 3% suspension. The resulted suspension was mixed with a magnetic stirrer at 400 rpm for 30 min. Afterwards, it was sonicated in an ultrasonic bath (Elmasonic E30H, Elma-Hans Schmidbauer GmbH & Co. KG, Germany) at a temperature of 50°C for 90 min to achieve the homogeneity of ZnO

nanoparticles in the solution. The same route was applied for the preparation of biosilica nanobiostructure suspension. Then, as-prepared ZnO nanoparticles suspension was added dropwise to the biosilica nanobiostructure suspension for 1 h under magnetic stirring. In a typical manner, the ZnO to biosilica mass ratio was set to 1:2. The resulted mixture was sonicated at a temperature of 50˚C for 120 min. Finally, the solid sample phase was separated through filtration and dried in an oven at 80˚C for 48 h.

2.3. Experimental setup

A batch flow mode cylindrical experimental reactor made of quartz with the working volume of 700 mL was used to evaluate the photocatalytic activity of ZnO nanostructures embedded in biosilica nanobiostructure. The reactor was surrounded by four 6-W low-pressure UVC lamps with the peak intensity at 254 nm (Philips, Holland). In the case of the comparative study, the visible light source was four 6-W visible lamps with the peak intensity at 544 nm. Magnetic stirring was applied to reach an efficient interaction between the photocatalyst and organic dye as the target pollutant. In a typical manner, 1 g/L of the photocatalyst was added into the solution containing the initial AR88 concentration of 20 mg/L within the stirring time of 30 min. Before starting the irradiation, the suspension was agitated in the dark for 20 min to reach adsorption/desorption equilibrium. After reaching the equilibrium time, the lamps were turned on.

2.4. Analysis

Field emission scanning electron microscopy (FE-SEM) was carried out by a TESCAN microscope (Mira3, Kohoutovice, Czech Republic) to characterize the surface morphology of the photocatalyst. To avoid charging during FE-SEM analysis, the samples were covered by a thin layer of gold film. In addition, Manual Microstructure Distance Measurement software (Nahamin Pardazan Asia Co., Iran) was employed to calculate diameter size distribution of the ZnO nanoparticles on the basis of one of the obtained FE-SEM images. The X-ray diffraction (XRD) patterns of the as-prepared photocatalyst were obtained by a PANalytical diffractometer (Model: X'Pert Pro MPD, the Netherlands) at $\lambda = 1.54056$ Å, step size = 0.026˚/s, scanning angle = 10–80˚, measurement temperature = 25˚C, voltage = 40 kV, and current intensity = 30 mA using anode material of Cu. Fourier transform infrared (FT-IR) analysis was also performed to evaluate the suitability of the immobilization process applied for the attachment of ZnO nanoparticles onto biosilica nanobiostructure. For the analysis, the KBr pellets were firstly prepared from the photocatalyst; then, FT-IR spectra were recorded using a spectrophotometer (Tensor 27, Bruker, Germany) in a wavenumber ranging from 400 to 4,000 cm^{-1}. UV–vis diffuse reflectance spectra (DRS) of the pure ZnO and ZnO/biosilica nanocomposite were recorded in a wavelength ranging from 200 to 1,000 nm in an Avantes spectrophotometer (Avaspec-2048-TEC, the Netherlands) using $BaSO_4$ as the standard sample. After the characterization of ZnO/biosilica nanocomposite, the experiments were carried out at evenly spaced intervals. After each run, 10 mL sample was withdrawn and centrifuged for 5 min at 4,400 min^{-1}. The resulted supernatant was used for measuring the residual concentration of AR88 via a UV–vis spectrophotometer (Hach, DR 5000, USA) at the maximum wavelength of 507 nm. The decolorization efficiency (%) of AR88 was computed via Eq. (3):

$$\text{Decolorization efficiency } (\%) = \left(1 - \left(\frac{C_t}{C_0}\right)\right) \times 100 \tag{3}$$

where C_0 and C_t are the concentrations of dye at time 0 and t, respectively. To confirm the mineralization of AR88 during the photocatalysis, chemical oxygen demand (COD) of the samples was measured using open reflux method [27]. Accordingly, the mineralization efficiency (%) was calculated by means of Eq. (4):

$$\text{Mineralization efficiency } (\%) = \left(1 - \left(\frac{\text{COD}_t}{\text{COD}_0}\right)\right) \times 100 \tag{4}$$

where COD_0 and COD_t are the values of COD at time 0 and t, respectively.

3. Results and discussion

3.1. Structural characteristics

3.1.1. FE-SEM results

FE-SEM analysis was carried out. The results are depicted in Fig. 1. The FE-SEM image of pure ZnO nanoparticles showed the good spherical shape of nanosized ZnO particles with some degree of aggregation (Fig. 1(a)). Besides, as shown in Fig. 1(a), the size distribution of ZnO nanoparticles was uniform and the particles had a relatively regular morphology. FE-SEM images of the immobilized form of ZnO nanoparticles are illustrated in Fig. 1(b) and (c). As it

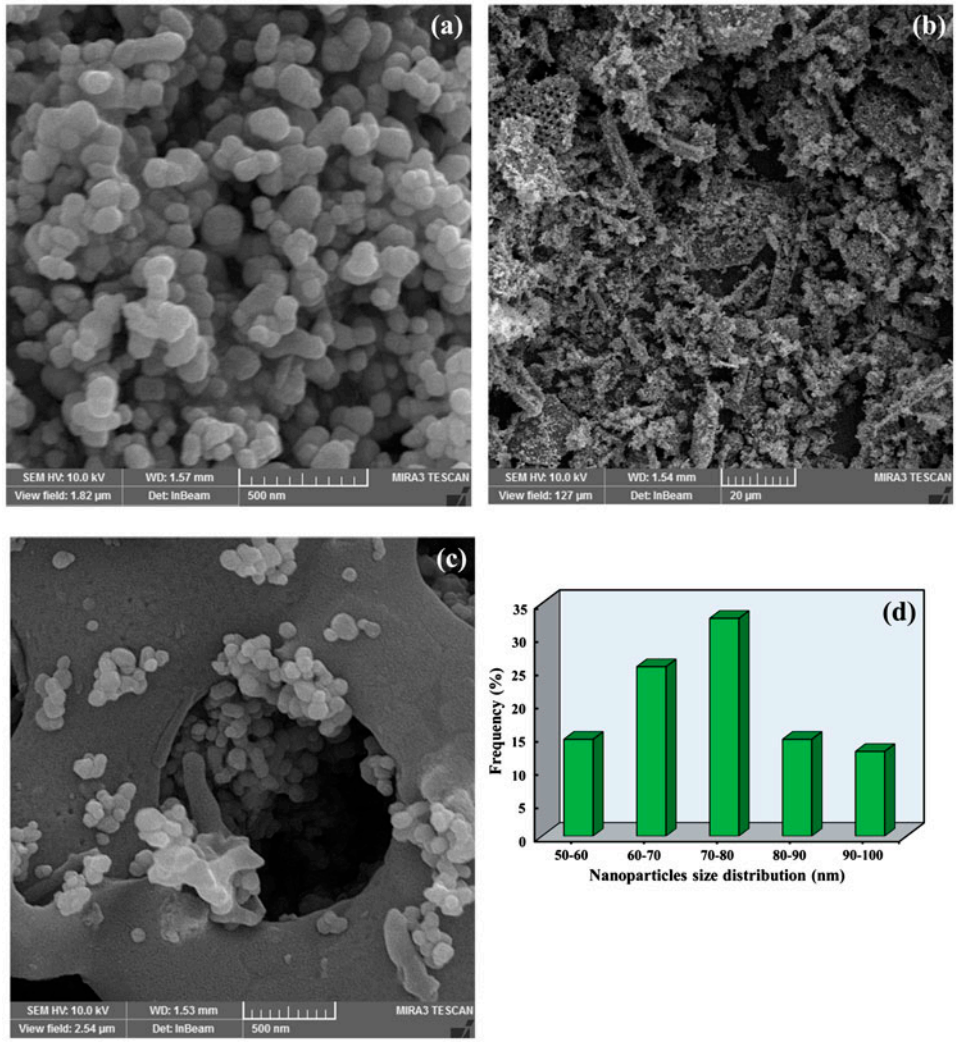

Fig. 1. SEM images of pure ZnO nanoparticles (a) and ZnO/biosilica nanocomposite (b and c) along with particle size distribution plot of ZnO nanoparticles (d).

is obvious, the immobilization of ZnO nanoparticles on biosilica nanobiostructure took place well. In addition, a relatively uniform distribution of ZnO nanoparticles on their support could be observed in Fig. 1(b). The pore structure of the support influenced the immobilization of ZnO nanoparticles due to the fact that the size exclusion limited the immobilization of the photocatalyst of a given particle size on the porous structure of the biosilica. As shown in Fig. 1(c), the pore diameter size of the biosilica was larger than that of ZnO. Therefore, ZnO nanoparticles could easily enter the pores of the biosilica and immobilize on its porous structure. This led to the uniform distribution of the particulate photocatalyst on the surface of support material. Additionally, the particle size distribution plot of ZnO nanoparticles was depicted using Manual Microstructure Distance Measurement software. As shown in Fig. 1(d), the average size of particles ranged from 50 to 100 nm and most of the particles were varied between 70 and 80 nm, with the frequency of 32.73%. The frequency of the range between 50 and 60 nm (as the smallest particle size range) was found to be 14.55%. As a result, most of the particles were ranged between 60 and 80 nm, with the frequency of about 60%, indicating the relatively uniform size distribution of ZnO nanoparticles.

3.1.2. XRD results

Fig. 2 shows the XRD patterns of pure biosilica nanobiostructure, pure ZnO nanoparticles, and ZnO/biosilica nanocomposite. The main dominant peaks

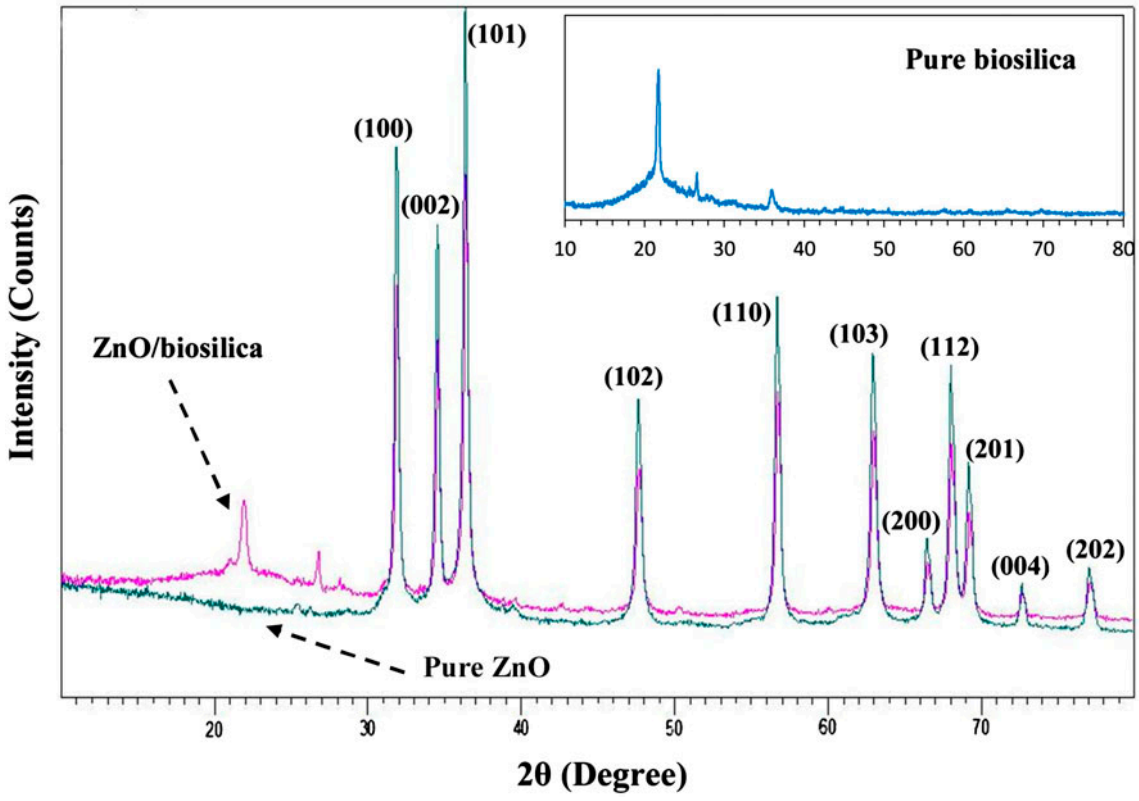

Fig. 2. XRD patterns of pure biosilica, pure ZnO nanoparticles, and ZnO/biosilica nanocomposite.

recognized for pure ZnO nanoparticles were at 2θ of 31.87˚, 34.55˚, 36.29˚, 47.57˚, 56.75˚, 62.89˚, 66.40˚, 68.09˚, 68.16˚, 72.51˚, and 76.98˚, which were attributed to the (1 0 0), (0 0 2), (1 0 1), (1 0 2), (1 1 0), (1 0 3), (2 0 0), (1 1 2), (2 0 1), (0 0 4), and (2 0 2) planes of hexagonal wurtzite ZnO nanoparticles, respectively (JCPDS Card 36-1451). A comparison of the XRD patterns revealed that the peak located at 2θ of 21.81 and 26.72˚ on the XRD pattern of the ZnO/biosilica nanocomposite was produced after the immobilization. This matched the major peaks of a pure phase of silica in the JCPDS Card 00-001-0647 [3], where biosilica was covered with pure ZnO nanoparticles. Diffraction values showed no shift to lower or higher angles in the case of ZnO/biosilica nanocomposite with respect to pure ZnO nanoparticles, thereby confirming that the immobilization of ZnO nanoparticles on biosilica did not affect the crystalline and chemical structure of pure ZnO nanoparticles. The crystalline size of as-prepared samples was determined using the Debye–Scherrer's equation as shown in Eq. (5) [28]:

$$D = \frac{0.9\lambda}{\beta \cos\theta} \quad (5)$$

where D is the crystalline size (Å), λ is the wavelength of the X-ray (Cu Kα = 1.54056 Å), θ is the diffraction angle, and β is the full width at half maximum (FWHM) intensity of the peak (rad). Accordingly, the average crystalline size for both pure ZnO nanoparticles and ZnO/biosilica nanocomposite was found to be about 40 nm.

3.1.3. FT-IR results

The functional groups placed on the surface of the photocatalyst play an important role during the photocatalysis due to the fact that the photocatalysis of target pollutant occurs on the surficial functional groups [16]. Therefore, in the present study, FT-IR analysis was conducted on biosilica alone and ZnO/biosilica nanocomposite in the range of 400–4,000 cm^{-1}. The results are shown in Fig. 3. The peak placed at 475 cm^{-1} was associated with Si–O–Si bond of the condensed silica network [29], which could be seen in both ZnO-loaded and unloaded biosilica nanobiostructure. The intensity of this peak was decreased and also shifted to 485 cm^{-1} after the immobilization of ZnO nanoparticles, thereby implying the significant role of

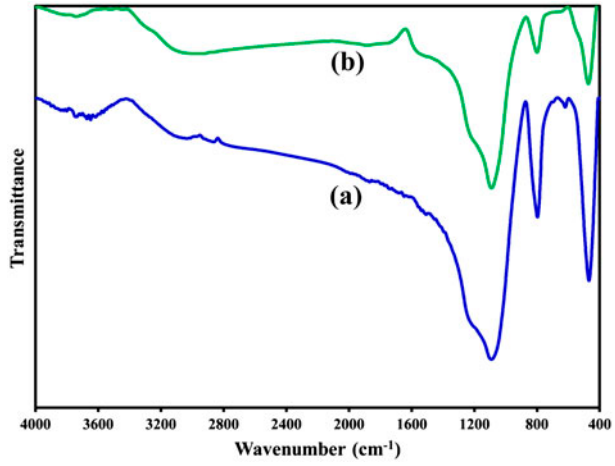

Fig. 3. FT-IR spectra of biosilica alone (a) and ZnO/biosilica nanocomposite (b).

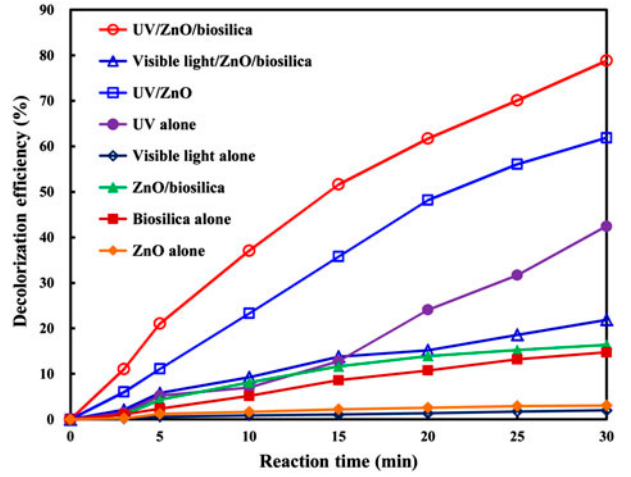

Fig. 4. Comparison between various processes involved in the photocatalysis of AR88.

this group in the immobilization process. As can be seen in Fig. 3, the intensity of the peak located at 800 cm^{-1} (associated with Si–O–Si bending) [30] was decreased after the immobilization of ZnO nanoparticles, confirming the involvement of this group of biosilica in the immobilization process. In addition, decreasing the intensity of the peak centered at 1,010 cm^{-1} (attributed to Si–O–Si stretching (in-plane) vibration for the layered silicates) [31] indicated the role of this group of biosilica in the immobilization process. Based on the results of FT-IR analysis, it could be concluded that the immobilization of ZnO on biosilica support was carried out well.

3.2. The role of each process involved in the photocatalysis

The effect of each process involved in the photocatalysis of AR88 was assessed. The results are shown in Fig. 4. In this set of experiments, the initial dye concentration, photocatalyst dosage, the initial pH, and the reaction time were set to 20 mg/L, 1 g/L, 7, and 30 min, respectively. Within a reaction time of 30 min, the decolorization efficiency of AR88 was obtained to be 3.07, 14.73, and 16.39% for ZnO alone, biosilica alone, and ZnO/biosilica nanocomposite, respectively. Therefore, the role of ZnO alone, biosilica alone, and their combination in the decolorization of AR88 through the adsorption mechanism was insignificant. Moreover, experiments with UV alone (photolysis) exhibited a decolorization efficiency of 42.44%. In the case of photocatalytic processes, as shown in Fig. 4, the photocatalytic decolorization of AR88 over pure ZnO nanoparticles was 61.86%, whereas the photocatalytic decolorization over ZnO/biosilica nanocomposite was 78.84%. Additionally, a simple comparison of the photocatalytic activity of UV-activated and visible light-activated ZnO/biosilica nanocomposite in the photocatalysis of AR88 was performed to evaluate the capability of as-prepared photocatalyst for treating colored solutions under visible light irradiation. As can be observed from Fig. 4, the photocatalytic decolorization efficiency (%) of AR88 over visible light-activated ZnO/biosilica nanocomposite was obtained to be 21.87%, which was lower than that obtained for the UV-activated ZnO/biosilica nanocomposite (78.84%). This indicated that visible light could not be used as an efficient and appropriate light source for the stimulation and subsequently, generation of hydroxyl radicals within a photoreactor. In addition, as shown in Fig. 4, the visible light alone had a negligible effect on the decolorization efficiency of AR88 within the specified reaction time. Obviously, the photocatalyst required a source light with sufficient energy (larger than band gap energy) to promote the transition of electrons from valence band to conduction band generating holes (h^+) and subsequently, hydroxyl radicals [32]. The results of the present work were in agreement with those obtained in our previous work [13]. As a result, the decolorization efficiency (%) of AR88 was increased in the order as follows: visible light alone < ZnO alone < biosilica alone < ZnO/biosilica < visible light/ZnO/biosilica < UV alone < UV/ZnO < UV/ZnO/biosilica. Although the amount of photocatalyst in ZnO/biosilica nanocomposite was lower than that of pure ZnO during the photocatalysis of AR88, the photocatalytic decolorization over ZnO/biosilica nanocomposite was greater than that over pure ZnO. This can be

associated with the decrease in the aggregation of photocatalyst nanoparticles within the solution, resulting in the effective absorption of photons generating hydroxyl radicals [20]. According to the above-mentioned results, the immobilization of ZnO nanoparticles on biosilica nanobiostructure increases the photocatalytic decolorization of AR88. It can be explained by the fact that the adsorption capacity of biosilica nanobiostructure improves the chance of hydroxyl radicals to degrade AR88. This means that the hydroxyl radicals generated on the surface of ZnO nanoparticles are easily transferred to the surface of ZnO/biosilica nanocomposite, which can degrade dye molecules adsorbed on the surface of support [11]. On the other hand, the ZnO nanoparticles act as photoactive centers for the generation of electron–hole pair, while the biosilica provides adsorptive sites in the vicinity of the photocatalyst. In accordance with the results of the present study, Fatimah et al. observed and reported that the immobilization of ZnO on the montmorillonite surface improved its photocatalytic activity in comparison with the pure ZnO [20]. In another study, de Brites-Nóbregaa et al. found that the synergic effect of ZnO and zeolite was higher than that of the activated charcoal [33]. The optical properties and consequently, the photocatalytic activity of pure ZnO and ZnO/biosilica nanocomposite were evaluated and compared by performing DRS analysis. The DRS of pure ZnO and ZnO/biosilica nanocomposite is exhibited in Fig. 5. As depicted, ZnO/biosilica nanocomposite had lower reflectance (%) than pure ZnO in the entire UV–vis light region. Therefore, the incorporation of ZnO nanoparticles into the biosilica structure increases the potential of nanocomposite to absorb further UV–vis light irradiation, leading to higher photocatalytic activity and subsequently, enhanced decolorization efficiency. In agreement to our results, Xu et al. reported that the ZnO/bentonite had a better utilization of both UV and visible light irradiation than pure ZnO [34]. Overall, the immobilization process leads to the consumption of lower amounts of photocatalyst in comparison with the application of pure photocatalyst, which increases the cost efficiency of the process.

3.3. The effect of photocatalyst dosage

In order to avoid the use of an excess amount of photocatalyst, it was essential to determine the optimum value for photocatalyst dosage in photocatalytic systems. Fig. 6 displays how the photocatalyst dosage influenced the photocatalytic decolorization of AR88. For this, the photocatalyst dosage was varied between 0.1 and 2 g/L, while the initial dye concentration, photocatalyst to biosilica ratio, the initial pH, and the reaction time were constant at 20 mg/L, 1:1, 7, and 30 min, respectively. As shown, with increasing the photocatalyst dosage from 0.1 to 1.5 g/L, the decolorization efficiency of AR88 was increased from 15.3 to 98.54%, respectively, while further increase in the amount of photocatalyst to 2 g/L led to a slight drop in the decolorization efficiency, decreasing to 93.63%. Similar results were reported by Muthirulan et al. in their study on the photocatalytic decolorization of alizarin cyanin green using immobilized ZnO [35]. Increasing the photocatalyst dosage provided higher surface area and active sites to adsorb UV light irradiation for the generation of hydroxyl radicals, while increasing the photocatalyst dosage up to a

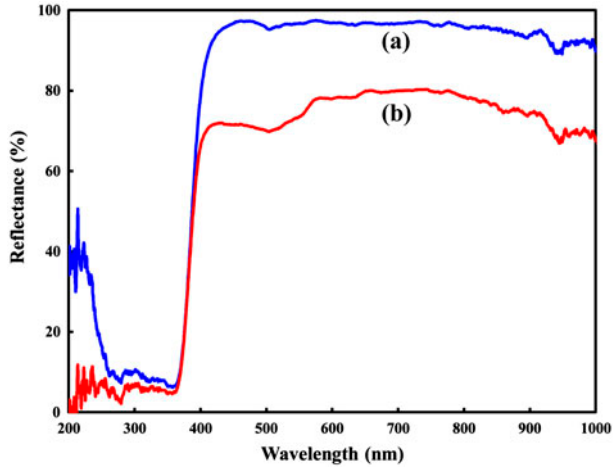

Fig. 5. UV–vis DRS spectra of the samples.

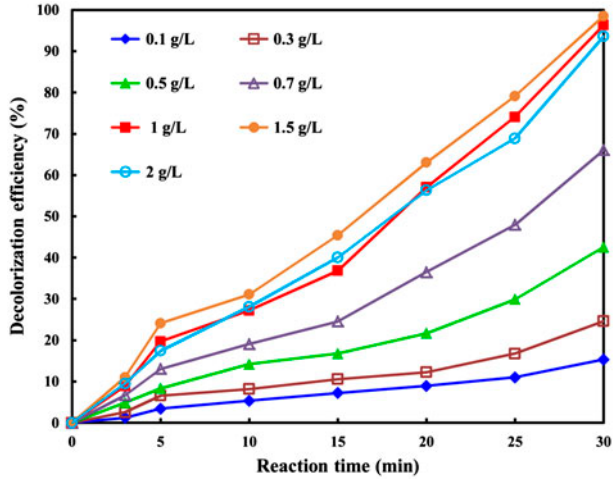

Fig. 6. The effect of photocatalyst dosage on the photocatalysis of AR88.

specific value created turbidity. A turbid solution can reduce light absorption and reflect light irradiation, thereby inhibiting the efficient generation of hydroxyl radical [20,36]. Therefore, the optimum value of photocatalyst dosage could lead to enhancing the photocatalytic decolorization of AR88 and avoiding the use of the excess amount of photocatalyst [2]. Accordingly, an optimal value of photocatalyst dosage had to be chosen to operate a photocatalytic process. For this, a photocatalyst dosage of 1 g/L was chosen as the optimal value for conducting the following experiments.

3.4. The effect of initial dye concentration

The effect of the initial AR88 concentration on its photocatalytic decolorization was investigated by varying the initial concentration between 10 and 70 mg/L (Fig. 7(a)). In this set of experiments, the values of photocatalyst dosage, ZnO to biosilica ratio, the initial pH, and the reaction time were set to 1 g/L, 1:1, 7, and 30 min, respectively. Decreasing the initial AR88 concentration from 70 to 20 mg/L enhanced its photocatalytic removal efficiency from 21.01 to 96.32%, respectively. At the initial AR88 concentration of 10 mg/L, the decolorization efficiency reached 100% within a short reaction time of 25 min. Clearly, the amount of $OH^{\bullet}$ needed for the degradation of dye molecules was increased as its initial concentration was enhanced. In addition, increasing the initial dye concentration diminished the path length of photons entering into the colored solution for exciting the active sites of the photocatalyst for the generation of hydroxyl radical [8,13]. Besides, with increasing the initial AR88 concentration, more and more organic dye molecules could be adsorbed on the photocatalyst surface; thus, the generation rate of $OH^{\bullet}$ could be reduced due to the presence of fewer active sites for the adsorption of UV light irradiation [36,37]. This led to the photolysis of dye molecules rather than the photocatalytic process, reducing the decolorization efficiency (%) of AR88. The photocatalytic decolorization of AR88 could be described by the pseudo-first-order kinetic Langmuir–Hinshelwood mechanism [9]. A plot of $\ln(C_0/C_t)$ vs. t was depicted to determine the apparent reaction rate constant (k_{ap}) as a function of the initial AR88 concentration. Accordingly, the linearized form of the plots (Fig. 7(b)) demonstrated that the decolorization reaction of AR88 followed the pseudo-first-order kinetic model. As plotted in Fig. 7(b), at initial AR88 concentrations of 10, 20, 30, 40, 50, and 70 mg/L, the apparent reaction rate constants (k_{ap}) were determined to be 0.1579, 0.0875, 0.0492, 0.0293, 0.0189, and 0.0078 min^{-1}, respectively. As a result, the photocatalytic decomposition rate was increased with decreasing the initial dye concentration. So, the photocatalytic decolorization of AR88 could be rather promising at low concentrations of the target pollutant. A similar trend was observed by Zhu et al. in their study on the photocatalytic degradation of an azo dye over immobilized ZnO [2]. To evaluate the cost efficiency of the photocatalytic process, EE_0 (kW h/m^3) of the photocatalytic decolorization of AR88, which defined as the number of kilowatt hours (kW h) of electrical energy needed to decrease the concentration of the target pollutant in 1 m^3 of solution by 1 order of magnitude (90%), was calculated through Eq. (6):

$$EE_0 = \frac{38.4 \times P}{V \times k_{obs}} \tag{6}$$

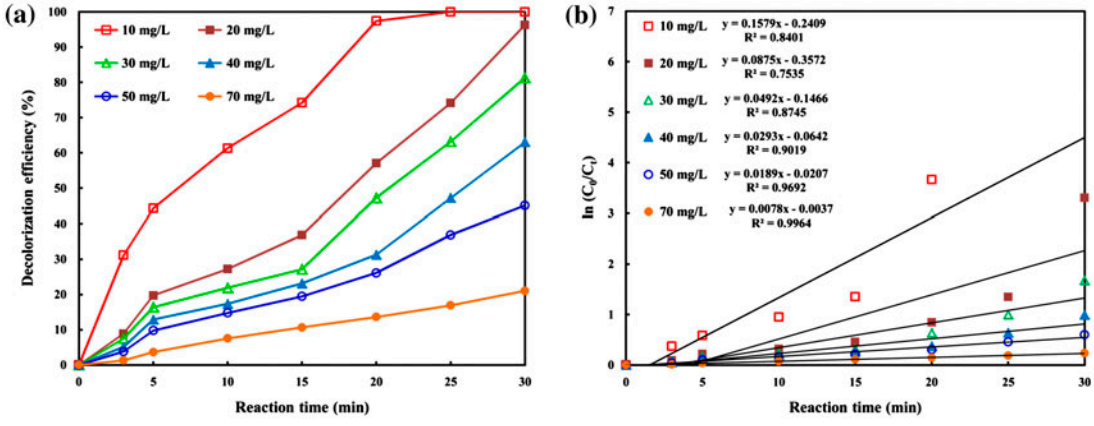

Fig. 7. The effect of initial AR88 concentration on its photocatalytic degradation (a), together with the corresponding kinetic plots (b).

where P, V, and k_{obs} are the rated power (kW), the apparent reaction rate constant (min^{-1}), and the volume (L) of the solution containing the target pollutant [31,38]. According to Eq. (10), the values of EE_0 at initial AR88 concentrations of 10, 20, 30, 40, 50, and 70 mg/L were obtained to be 139, 251, 446, 749, 1,161, and 2,813 kW h/m^3, respectively. It can be stated that increasing the initial concentration of AR88 resulted in the higher consumption of electrical energy per unit volume of the reactor. The above-mentioned information could be beneficial to determine the energy required for the photocatalytic decolorization of organic dyes from an application viewpoint.

3.5. Reusability evaluation

The recycling of as-prepared photocatalytic is a key issue concerning long-term application of the photocatalyst. The reusability test was performed using 0.1 M H_2SO_4 as the chemical reagent within a reaction time of 30 min to attain chemical regeneration of the spent photocatalyst, while photocatalyst dosage, the initial dye concentration, ZnO/biosilica ratio, and the initial pH were constant at 1 g/L, 20 mg/L, 1:1, and 7, respectively. Four consecutive experimental runs were carried out to specify the loss in the decolorization efficiency of AR88 after each reuse. The results of reusability test are depicted in Fig. 8. As shown, the decolorization efficiency of AR88 at the first, second, third, and fourth experimental run was 96.32, 94.05, 93.12, and 89.47%, respectively. As a result, the ZnO/biosilica nanocomposite did not show any significant loss of photocatalytic activity after four cycles. Thus, ZnO/biosilica nanocomposite could be used as an efficient photocatalyst with high reusability potential. This could be due to the stability of as-prepared ZnO/biosilica nanocomposite. The porous structure and also the surficial active sites in the clay-like support stabilize ZnO nanoparticles and consequently, prevent their release into the solution [33]. This means that the photocatalytic decolorization of AR88 can be operated as an economically feasible and environmentally friendly method with a relatively low cost. Similar results have been reported by Li and colleagues in the case of the photocatalytic decolorization of methylene blue over ZnO/rectorite composite [24]. A little drop in the decolorization efficiency of AR88 within four consecutive experimental runs could be due to the loss of ZnO from the biosilica surface and the fouling of the photocatalyst by the byproducts generated during the photocatalytic degradation of AR88 [39].

3.6. Mineralization test

To evaluate the potential of UV light-activated ZnO/biosilica nanobiocomposite in mineralizing dye molecules, COD of the colored solution before and after the photocatalysis was measured at an initial dye concentration of 20 mg/L within a reaction time of 30 min. It could be a suitable way to determine the progress in mineralization during the photocatalysis of various organic target pollutants such as organic dyes due to the fact that COD analysis is a measure of the oxygen equivalent of the organic compound that can be oxidized chemically to CO_2 and H_2O [9,11,38]. Fig. 9 exhibits a mineralization efficiency of 65.57%, while the decolorization efficiency reached to 96.32% at the same experimental conditions. The obtained

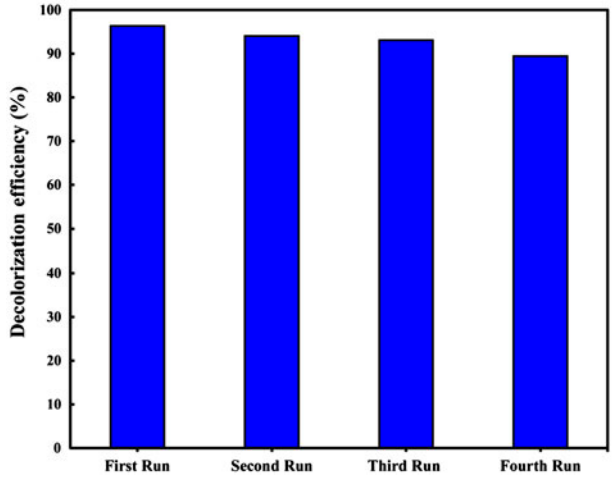

Fig. 8. Reusability of the ZnO/biosilica nanocomposite within four experimental runs.

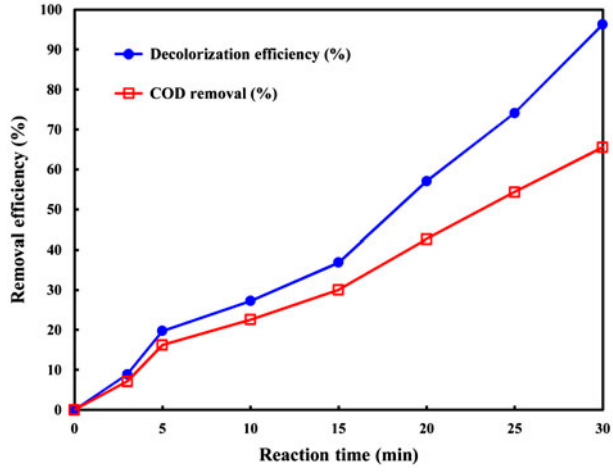

Fig. 9. Mineralization of AR88 in the presence of ZnO/biosilica nanocomposite.

results confirmed an acceptable mineralization of AR88 within a short reaction time of 30 min. This indicated the low production of long-lived byproducts with low k_{ap} to react with photogenerated hydroxyl radicals [9].

4. Conclusions

Nanostructured ZnO was immobilized onto a siliceous material named biosilica to be used as an efficient and reusable photocatalyst for the degradation of a textile dye in aqueous solutions. SEM, XRD, and FT-IR analysis indicated that the immobilization of ZnO nanoparticles was carried out reasonably well. As a result, the photocatalytic activity of immobilized ZnO was higher than that of pure ZnO. This was confirmed by the obtained UV–vis DRS. Besides, visible light irradiation could not be considered as an appropriate light source for the photocatalysis of target pollutant within a short reaction time. Increasing the photocatalyst dosage, along with decreasing initial dye concentration, favored the photocatalytic decolorization efficiency (%). Increasing initial AR88 concentration resulted in the higher consumption of electrical energy per unit volume of the reactor. The results of reusability test also demonstrated the high potential of as-prepared photocatalyst as a reliable alternative in full-scale applications. In addition, the reduction of COD was substantial in comparison with the decolorization. Overall, ZnO/biosilica nanocomposite can be a suitable combination for the photocatalytic degradation of organic dyes.

Acknowledgments

The authors gratefully appreciate the financial support of the Iran National Science Foundation (INSF) (Grant no. 92023339). The authors also wish to thank Arak University of Medical Sciences (Iran) for instrumental supports.

References

[1] Z. Noorimotlagh, R. Darvishi Cheshmeh Soltani, A.R. Khataee, S. Shahriyar, H. Nourmoradi, Adsorption of a textile dye in aqueous phase using mesoporous activated carbon prepared from Iranian milk vetch, J. Taiwan Inst. Chem. Eng. 45 (2014) 1783–1791.

[2] H.-Y. Zhu, L. Xiao, R. Jiang, G.-M. Zeng, L. Liu, Efficient decolorization of azo dye solution by visible light-induced photocatalytic process using SnO_2/ZnO heterojunction immobilized in chitosan matrix, Chem. Eng. J. 172 (2011) 746–753.

[3] R. Darvishi Cheshmeh Soltani, A.R. Khataee, M. Safari, S.W. Joo, Preparation of bio-silica/chitosan nanocomposite for adsorption of a textile dye in aqueous solutions, Int. Biodeterior. Biodegrad. 85 (2013) 383–391.

[4] R. Darvishi Cheshmeh Soltani, A.R. Khataee, H. Godini, M. Safari, M.J. Ghanadzadeh, M.S. Rajaei, Response surface methodological evaluation of the adsorption of textile dye onto biosilica/alginate nanobiocomposite: Thermodynamic, kinetic, and isotherm studies, Desalin. Water Treat. (in press), doi: 10.1080/19443994.2014.950344.

[5] S.-M. Lam, J.-C. Sin, A.Z. Abdullah, A.R. Mohamed, Degradation of wastewaters containing organic dyes photocatalysed by zinc oxide: A review, Desalin. Water Treat. 41 (2012) 131–169.

[6] M.S. Lucas, P.B. Tavares, J.A. Peres, J.L. Faria, M. Rocha, C. Pereira, C. Freire, Photocatalytic degradation of Reactive Black 5 with TiO_2-coated magnetic nanoparticles, Catal. Today 209 (2013) 116–121.

[7] M.H. Dehghani, P. Mahdavi, Removal of acid 4092 dye from aqueous solution by zinc oxide nanoparticles and ultraviolet irradiation, Desalin. Water Treat. 54 (2015) 3464–3469.

[8] R. Darvishi Cheshmeh Soltani, A. Rezaee, A.R. Khataee, M. Safari, Photocatalytic process by immobilized carbon black/ZnO nanocomposite for dye removal from aqueous medium: Optimization by response surface methodology, J. Ind. Eng. Chem. 20 (2014) 1861–1868.

[9] R. Darvishi Cheshmeh Soltani, A. Rezaee, M. Safari, A.R. Khataee, B. Karimi, Photocatalytic degradation of formaldehyde in aqueous solution using ZnO nanoparticles immobilized on glass plates, Desalin. Water Treat. 53 (2015) 1613–1620.

[10] B. Karimi, M.-S. Rajaei, A. Koulivand, R.D. Cheshmeh Soltani, Performance evaluation of advanced Fe°/Fe^{2+}/Fe^{3+}/H_2O_2 process in the reduction of nitrate and organic matter from aqueous solution, Desalin. Water Treat. 52 (2013) 6240–6248.

[11] A. Nezamzadeh-Ejhieh, S. Khorsandi, Photocatalytic degradation of 4-nitrophenol with ZnO supported nano-clinoptilolite zeolite, J. Ind. Eng. Chem. 20 (2014) 937–946.

[12] A. Khataee, A. Karimi, S. Arefi-Oskoui, R. Darvishi Cheshmeh Soltani, Y. Hanifehpour, B. Soltani, S.W. Joo, Sonochemical synthesis of Pr-doped ZnO nanoparticles for sonocatalytic degradation of Acid Red 17, Ultrason. Sonochem. 22 (2015) 371–381.

[13] A. Khataee, R. Darvishi Cheshmeh Soltani, Y. Hanifehpour, M. Safarpour, H. Gholipour Ranjbar, S.W. Joo, Synthesis and characterization of dysprosium-doped ZnO nanoparticles for photocatalysis of a textile dye under visible light irradiation, Ind. Eng. Chem. Res. 53 (2014) 1924–1932.

[14] S. Meshram, R. Limaye, S. Ghodke, S. Nigam, S. Sonawane, R. Chikate, Continuous flow photocatalytic reactor using ZnO–bentonite nanocomposite for degradation of phenol, Chem. Eng. J. 172 (2011) 1008–1015.

[15] A. Rezaee, H. Masoumbaigi, R. Darvishi Cheshmeh Soltani, A.R. Khataee, S. Hashemiyan, Photocatalytic decolorization of methylene blue using immobilized ZnO nanoparticles prepared by solution combustion method, Desalin. Water Treat. 44 (2012) 174–179.

[16] R. Darvishi Cheshmeh Soltani, A. Rezaee, A. Khataee, Combination of carbon black-ZnO/UV process with an electrochemical process equipped with a carbon black-PTFE-coated gas-diffusion cathode for removal of a textile dye, Ind. Eng. Chem. Res. 52 (2013) 14133–14142.
[17] H. Wang, R.L. Wick, B. Xing, Toxicity of nanoparticulate and bulk ZnO, Al_2O_3 and TiO_2 to the nematode *Caenorhabditis elegans*, Environ. Pollut. 157 (2009) 1171–1177.
[18] K. Aschberger, C. Micheletti, B. Sokull-Klüttgen, F.M. Christensen, Analysis of currently available data for characterising the risk of engineered nanomaterials to the environment and human health—Lessons learned from four case studies, Environ. Int. 37 (2011) 1143–1156.
[19] C. Som, P. Wick, H. Krug, B. Nowack, Environmental and health effects of nanomaterials in nanotextiles and façade coatings, Environ. Int. 37 (2011) 1131–1142.
[20] I. Fatimah, S. Wang, D. Wulandari, ZnO/montmorillonite for photocatalytic and photochemical degradation of methylene blue, Appl. Clay Sci. 53 (2011) 553–560.
[21] H.Y. Zhu, R. Jiang, Y.Q. Fu, J.H. Jiang, L. Xiao, G.M. Zeng, Preparation, characterization and dye adsorption properties of γ-Fe_2O_3/SiO_2/chitosan composite, Appl. Surf. Sci. 258 (2011) 1337–1344.
[22] M. Habibi, A.A.L. Zinatizadeh, M. Akia, Photocatalytic degradation of Tire Cord manufacturing wastewater using an immobilized nanoTiO_2 photocatalytic reactor, Desalin. Water Treat. (in press), doi: 10.1080/19443994.2014.979328.
[23] Y. Jia, W. Han, G. Xiong, W. Yang, Layer-by-layer assembly of TiO_2 colloids onto diatomite to build hierarchical porous materials, J. Colloid Interface Sci. 323 (2008) 326–331.
[24] S.-Q. Li, P.-J. Zhou, W.-S. Zhang, S. Chen, H. Peng, Effective photocatalytic decolorization of methylene blue utilizing ZnO/rectorite nanocomposite under simulated solar irradiation, J. Alloys Compd. 616 (2014) 227–234.
[25] K. Mamulová Kutláková, J. Tokarský, P. Peikertová, Functional and eco-friendly nanocomposite kaolinite/ZnO with high photocatalytic activity, Appl. Catal., B 162 (2015) 392–400.
[26] S.P. Patil, V.S. Shrivastava, G.H. Sonawane, Photocatalytic degradation of Rhodamine 6G using ZnO-montmorillonite nanocomposite: A kinetic approach, Desalin. Water Treat. 54 (2014) 374–381.
[27] APHA, AWWA, WEF, Standard Methods for the Examination of Water and Wastewater, American Public Health Association, Washington, DC, 2005.
[28] A.L. Patterson, The Scherrer formula for X-ray particle size determination, Phys. Rev. 56 (1939) 978–982.
[29] M. Zarezadeh-Mehrizi, A. Badiei, A.R. Mehrabadi, Ionic liquid functionalized nanoporous silica for removal of anionic dye, J. Mol. Liq. 180 (2013) 95–100.
[30] M.-C. Wu, J.J.P. Coca, G.R.-L. Chang, S.-Y. Suen, C.-F. Lin, H.-N. Chou, S.-Y. Lai, M.-Y. Wang, Chemical modification of Nitzschia panduriformis's frustules for protein and viral nanoparticle adsorption, Process Biochem. 47 (2012) 2204–2210.
[31] M. Shirzad-Siboni, M. Farrokhi, R. Darvishi Cheshmeh Soltani, A. Khataee, S. Tajassosi, Photocatalytic reduction of hexavalent Chromium over ZnO nanorods immobilized on kaolin, Ind. Eng. Chem. Res. 53 (2014) 1079–1087.
[32] T.A. Saleh, M.A. Gondal, Q.A. Drmosh, Z.H. Yamani, A. AL-yamani, Enhancement in photocatalytic activity for acetaldehyde removal by embedding ZnO nano particles on multiwall carbon nanotubes, Chem. Eng. J. 166 (2011) 407–412.
[33] A. Dhakshinamoorthy, P. Visuvamithiran, V. Tharmaraj, K. Pitchumani, Clay encapsulated ZnO nanoparticles as efficient catalysts for N-benzylation of amines, Catal. Commun. 16 (2011) 15–19.
[34] H. Xu, T. Yu, J. Liu, Photo-degradation of Acid Yellow 11 in aqueous on nano-ZnO/bentonite under ultraviolet and visible light irradiation, Mater. Lett. 117 (2014) 263–265.
[35] P. Muthirulan, M. Meenakshisundararam, N. Kannan, Beneficial role of ZnO photocatalyst supported with porous activated carbon for the mineralization of alizarin cyanin green dye in aqueous solution, J. Adv. Res. 4 (2013) 479–484.
[36] N. Sobana, B. Krishnakumar, M. Swaminathan, Synergism and effect of operational parameters on solar photocatalytic degradation of an azo dye (Direct Yellow 4) using activated carbon-loaded zinc oxide, Mater. Sci. Semicond. Process. 16 (2013) 1046–1051.
[37] M.A. Behnajady, S.G. Moghaddam, N. Modirshahla, M. Shokri, Investigation of the effect of heat attachment method parameters at photocatalytic activity of immobilized ZnO nanoparticles on glass plate, Desalination 249 (2009) 1371–1376.
[38] G. Tchobanoglous, F.L. Burton, H.D. Stensel, Wastewater Engineering: Treatment and Reuse, Mc Graw-Hill, New York, NY, 2003.
[39] A. Nezamzadeh-Ejhieh, M. Karimi-Shamsabadi, Comparison of photocatalytic efficiency of supported CuO onto micro and nano particles of zeolite X in photodecolorization of Methylene blue and Methyl orange aqueous mixture, Appl. Catal., A 477 (2014) 83–92.